

Thermorheological behavior of polyethylene: a sensitive probe to molecular structure

Julia A. Resch · Ute Keßner · Florian J. Stadler

Received: 30 March 2011 / Revised: 5 June 2011 / Accepted: 23 June 2011 / Published online: 30 July 2011
© Springer-Verlag 2011

Abstract Recent investigations have shown that different topographies in polyethylene (PE) lead to either thermorheological simplicity (linear and short-chain branched PE) or two different types of thermorheologically complex behavior. Low-density polyethylene (LDPE) has a thermorheological complexity, which can be eliminated by a modulus shift, while long-chain branched metallocene PE (LCB-mPE) has a temperature dependent shape of the spectrum and thus a total failure of the time-temperature superposition principle. The reason for that behavior lies in the different relaxation times of linear and long-chain branched chains, present in LCB-mPE. The origin of the thermorheological complexity of LDPE might be the temperature dependence of the

miscibility of the different molar mass fractions that differ in their content of short chain branches.

Keywords Polyethylene · Thermorheological complexity · Molecular architecture · Activation energy

Introduction

Polyethylene (PE) is the most used polymer worldwide. While some aspects of it are relatively well understood nowadays, many aspects remain illusive despite the fact that PE is the simplest polymer available (Dealy and Larson 2006). There are three main types of PE, which differ by their short- and long-chain branching topography: high-density polyethylene (HDPE; Natta 1963; Ziegler 1963) produced in a catalytic process having no or very little side chains, low-density polyethylene (LDPE; Fawcett et al. 1937) produced in a high pressure process having many short- and long-chain branches, and linear low-density polyethylene (LLDPE) being produced like HDPE but with comonomers added leading to many short- but no or very few long-chain branches. The development of metallocene catalysts (Brant et al. 1994; Lai et al. 1993) led to the large-scale production of well-defined polyethylenes with a narrow molar mass distribution ($M_w/M_n = 2$) in combination with co-catalysts such as methylaluminoxane (Sinn and Kaminsky 1980).

Metallocene catalysts have the ability to polymerize not only short vinyl-terminated chains but also longer α -olefins, which the older and less defined Ziegler-Natta or Chromium catalysts (Natta 1963; Ziegler 1963) cannot. This enables them to reincorporate

This paper is dedicated to Professor Helmut Münstedt, Friedrich-Alexander Universität Erlangen-Nürnberg on the occasion of his 70th birthday.

J. A. Resch · U. Keßner · F. J. Stadler
Institute of Polymer Materials, Friedrich-Alexander
University Erlangen-Nürnberg, Martensstr. 7,
91058 Erlangen, Germany

J. A. Resch
Senoplast Klepsch & Co. GmbH, Wilhelm-Klepsch-Str. 1,
5721 Piesendorf, Austria

U. Keßner
BASF Coatings GmbH, GKD/MAR,
Rheology/Thermal Analysis, 48165 Münster, Germany

F. J. Stadler (✉)
School of Semiconductor and Chemical Engineering,
Chonbuk National University, Baekjero 567, Deokjin-gu,
Jeonju, Jeonbuk, 561-756, Republic of Korea
e-mail: fjstadler@jbnu.ac.kr

vinyl-terminated polyethylene chains into a growing chain and, thus, to form long-chain branches, which has proven to improve the processing properties of this material class significantly (e.g., Münstedt et al. 2005). As a general rule, it can be said that the higher the long-chain branching content, the higher is the strain hardening; thus, the better is the processing of elongation dominated processes (Hepperle and Münstedt 2006; Meissner 1969; Meissner and Hostettler 1994; Meissner et al. 1982; Münstedt et al. 2005; Stadler et al. 2009; Stange et al. 2005).

Besides the positive influence on the processing properties, long-chain branches also distinctly increase the activation energy, if an Arrhenius-type behavior dominates (Carella et al. 1986; Lohse et al. 2002). A WLF-type temperature dependence stays unaffected by the chain architecture, however (Hepperle et al. 2005; Kapnistos et al. 2005).

In polyethylene, it has been reported that long-chain branching leads to thermorheological complexity. Jacovic et al. (1979), Laun (1987), Rokudai and Fujiki (1981), Verser and Maxwell (1970) found for LDPE that the activation energy of the viscosity function $\eta(\dot{\gamma})$ decreases from about 57 kJ/mol to about 30 kJ/mol at the highest shear rates, while HDPE shows a constant activation energy as a function of $\dot{\gamma}$. This finding was recently confirmed by Keßner et al. (2009).

Based on the observation that the viscoelastic data of LDPE cannot be shifted to a master curve along the time/frequency axis alone, Mavridis and Shroff (1992) developed the concept of a vertical shift (a shift along the modulus axis), from which they calculated a vertical activation energy E_v . This is possible, because the shape of the viscoelastic functions as a function of angular frequency is independent of the temperature and only shifted along the modulus axis.

However, the physical background of such vertical activation energy was neither given by Mavridis and Shroff (1992), except that it will lead to a change in the entanglement molar mass M_e , nor is it logical from a physics point of view. The Arrhenius law (1916) can only describe temperature dependencies of a characteristic time, rate, or frequency. Hence, it is not possible to apply a time–temperature-dependence law to modulus–temperature-dependence, as a modulus—a priori—does not have a time component (however, this does not mean that a modulus has to be time-independent). Hence, the vertical activation energy E_v calculated from a modulus shift lacks any physical background.

For long-chain branched metallocene catalyzed PE (LCB-mPE), Wood-Adams and Costeux (2001) and Stadler et al. (2008) found that this class of poly-

mers cannot be shifted onto a master curve by a two-dimensional minimization, as the shape of the viscoelastic functions, especially $G'(\omega)$, $\delta(\omega)$, and $\delta(|G^*|)$, are temperature dependent. Stange et al. (2007) found a very similar behavior for slightly long-chain branched THV, essentially a semi-fluorinated ethylene-propylene copolymer, whose long-chain branching topography is similar to LCB-mPE. Hence, this similarity indicates a generality for the influence of long-chain branches on the thermorheological behavior of materials with an Arrhenius temperature dependence.

The analysis of the thermorheological complexity in LCB-mPE was performed by determining the shift factors as a function of modulus Wood-Adams and Costeux (2001) and relaxation strength (Stadler et al. 2008) using a special method for the calculation of relaxation spectra allowing for a greater mode density than in conventional spectra calculation routines (Kaschta and Stadler 2009).

Resch et al. (2009) found for LCB-mPE using creep and creep recovery tests that the thermorheological complexity is not only present in dynamic-mechanical tests but also in this—rather rarely used—experimental mode. While the creep compliance can be used relatively well to create a master curve, which fits the long time but not the short time data sufficiently, the creep recovery compliance $J_r(t)$ cannot be used for a master curve at all. Instead, it was found that the terminal value of the creep recovery compliance, the steady-state elastic recovery compliance J_e^0 decreases by a factor of up to 5 with increasing temperature. For LDPE, this effect is smaller, while for linear PE, J_e^0 is constant within the experimental accuracy. Hence, J_e^0 is related to the thermorheological behavior as well and can be used as an indicator for it.

These findings seem to be highly confusing at a first glance. This article will shed some light into this rather complicated issue based on the interpretation of relaxation spectra to gain some insight into the branching architecture and how it correlates with the thermorheological behavior. The ultimate aim is to establish an overview how different kinds of molecular architecture in PE differ in their architecture, which then can be used in the future to tailor new grades to specific behavior.

Experimental

The data used in this paper were partially published previously by Keßner et al. (2009), Resch et al. (2009), Stadler et al. (2005, 2007, 2008), Stadler and Münstedt (2008a).

All materials except for F18F and B13P are commercially available products. F18F was synthesized by Piel et al. (2006a) and B13P by Burcak Arikon-Conley (material unpublished so far, synthesis conditions identical to B4 (Piel et al. 2006b), except that a 50/50 mixture of ethene and propene was used for the synthesis of B13P (B4: pure ethene)), both group of Prof. Kaminsky, University Hamburg.

The molecular and rheological properties are summarized in Table 1.

SEC-MALLS

Molar mass measurements were carried out using a high temperature size exclusion chromatograph (Waters, 150C) equipped with refractive index (RI) and infrared (IR) (PolyChar, IR4) detectors. All measurements were taken at 140°C using 1,2,4-trichlorobenzene as the solvent. The high-temperature SEC was coupled with a multi-angle laser light scattering (MALLS) apparatus (Wyatt, DAWN EOS). Details of the experimental SEC-MALLS setup and measuring conditions are described by Stadler et al. (2006).

The SEC-MALLS data are given in the tables as the weight average molar mass M_w , polydispersity index M_w/M_n , and if applicable, the degree of branching calculated from the coil contraction according to Zimm-Stockmayer-theory (Zimm and Stockmayer 1949).

Rheology

The samples were compression molded into circular discs of 25 mm in diameter and between 1 and 2 mm in height. Antioxidative stabilizers (0.5 wt.% Irganox 1010 and 0.5 wt.% Irgafos 38 (Ciba SC)) were added to the laboratory scale samples. The commercial mPEs were sufficiently stable without an additional stabilizer. More details are given elsewhere (Stadler et al. 2006).

Shear rheological tests were carried out at various, constant temperatures between 130°C and 230°C in a nitrogen atmosphere. The tests were carried out using a Bohlin/Malvern Gemini and a TA Instruments AR-G2. Dynamic-mechanical tests (frequency sweeps) were carried out in the linear viscoelastic regime between frequencies ω of 1,000 and 0.01 s⁻¹. Typically oscillatory stresses with amplitudes τ_0 between 10 and 100 Pa or deformation amplitudes γ_0 of approximately 5% were applied depending on the viscosity of the sample. The thermal stability was measured by conducting a frequency sweep after loading the sample and repeating the same test after longer creep and creep-recovery tests, which took up to 3 days per measurement.

Table 1 Molecular and rheological data

Material	Type	M_w [kg/mol]	M_w/M_n [-]	Comonomer	T_m [°C]	η_0 (T= 150°C) [Pa s]	η_0/η_0^{lin} (T= 150°C) [-]	J_e^0 (T= 150°C) [Pa ⁻¹]	LCBR	LCB _{SEC}
L6	mLLDPE	114	1.9	Hexene	99	13800	0.96	$3.35 \pm 0.1 \times 10^{-5}$	None	None
L6-2		108	3.1	Hexene	108	16400	0.8	$4.63 \pm 0.52 \times 10^{-5}$	None	None
F18F		216	2.1	Octadecene	104	145800	0.99	$3.4 \pm 0.4 \times 10^{-4}$	None	None
B13P	LCB-mLLDPE	65	2	Propene	n.d.	5700	2.8	$> 2.3 \times 10^{-4}$	Star-like	Few
LB 1		94	2.2	Octene	101	33100	4.6	$5.08 \pm 0.22 \times 10^{-4}$	Star-like	Few
LB 4		85	2.3	Octene	106	44500	8.9	$4.50 \pm 0.06 \times 10^{-4}$	Star-like	Few
LDPE 1	LDPE	350	19	-	110	474000	0.6	$1.28 \pm 0.06 \times 10^{-3}$	Tree-like	Very high
LDPE 2		230	13.7	-	110	44500	0.25	$7.35 \pm 0.06 \times 10^{-4}$	Tree-like	Very high
LDPE 3		150	12	-	107	2560	0.07	$4.18 \pm 0.08 \times 10^{-4}$	Tree-like	Very high
LDPE 4		213	23	-	109	60150	0.3	$1.10 \pm 0.03 \times 10^{-3}$	Tree-like	Very high

§No steady-state value of the elastic recovery compliance could be determined
mLLDPE metallocene catalyzed linear low density polyethylene, LCB-mLLDPE long-chain branched metallocene catalyzed linear low density polyethylene, LDPE low-density polyethylene

Creep and creep-recovery tests were performed to determine the zero shear-rate viscosity η_0 from the creep compliance $J(t')$ by

$$\log \eta_0 = \lim_{t' \rightarrow \infty} \left(\log \left(\frac{t'}{J} \right) \right). \quad (1)$$

The linear steady-state elastic compliance J_e^0 was determined from the elastic (creep-recovery) compliance $J_r(t)$ by

$$J_e^0 = \lim_{t, t' \rightarrow \infty} J_r(t). \quad (2)$$

The linearity and stationarity was ensured for all creep and creep-recovery tests (for the precise methods and further experimental requirements to properly perform such tests see Gabriel et al. 1998). Typically creep stresses τ between 2 and 50 Pa were applied depending on the viscosity of the sample. Examples of creep and creep-recovery tests are given in Fig. 1. For very long creep times, the creep compliance reaches a constant slope of 1, which is equal to a plateau in t'/J (Eq. 1). At very long recovery times, the elastic recoverable compliance $J_r(t)$ reaches a plateau, which is the *linear steady-state elastic compliance* J_e^0 .

The relaxation spectra were then calculated from the combined data of frequency sweeps and creep-recovery tests (Kaschta and Schwarzl 1994a, b) using the method of Stadler (2010), Stadler and Bailly (2009), which was developed partially based on the method of Kaschta and Stadler (2009) to yield an even greater precision.

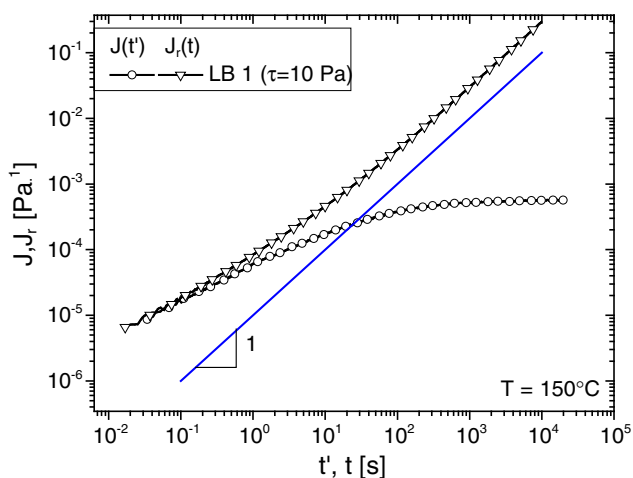


Fig. 1 Examples of the creep and creep-recovery tests for sample LB 1

Results

How can thermorheological complexity be detected?

For determining thermorheological complexity, different practices are known from literature. The most common method is the temperature superposition in the time or frequency domain of rheological quantities. $G'(\omega)$ and $G''(\omega)$ are mostly used for the analysis in literature.

However, the detection of thermorheological complexity from the master curves of $G'(\omega \times a_T)$ and $G''(\omega \times a_T)$ is not always easy, as small differences may be masked by the large scale of the plot (see Fig. 2). Figure 2b shows that a shift based on the region around the crossover leads to a small deviation in the terminal and the high frequency regime, which, however, requires very good experiments and a very wide range of angular frequencies (5–8 decades in frequency at four temperatures or more). Both conditions, however, are rarely fulfilled in literature, as the standard is rather 3–4 decades in frequency at 3 temperatures.

When only looking at the angular frequencies ω between 628 and 0.1 s^{-1} , almost no thermorheological complexity is present in the logarithmic plots (Fig. 2a, b). The data in Fig. 2b was shifted to form a “pseudo-master curve” by global minimization.

A linear plot of $G'(\omega)$ (Fig. 2c, open symbols) and $G''(\omega)$ discussed by Stadler et al. (2008) previously, highlights the thermorheological complexity somewhat, but is not totally satisfactory.

A clear disadvantage of the linear plot is that the thermorheological complexity might be hidden when choosing shifting with a high priority on the high frequencies (or moduli). This is demonstrated in the shifted curves of Fig. 2c (filled symbols), where the shift factors were optimized for the highest moduli of around 4×10^5 Pa, instead of 10^5 Pa, i.e., around ω_c (please note that for the sake of clarity the 2×10^5 Pa was added to the value of $G'(\omega)$). In this case, an almost perfect master curve is obvious. Hence, using the linear plot is only useful when shifting to obtain a perfect fit at the low frequencies or using a global minimization on logarithmic scale, as this will make differences between different temperatures larger at the high frequencies.

For this reason, $G'(\omega)$ and $G''(\omega)$ are not the best choice for analyzing a thermorheological complexity. Furthermore, detecting a thermorheological complexity might not be easily possible, if the deviation from the simple behavior is small. Hence, more suitable linear viscoelastic quantities are discussed in the following.

van Gorp and Palmen (1998) proposed the plot of the phase angle as a function of the absolute value of

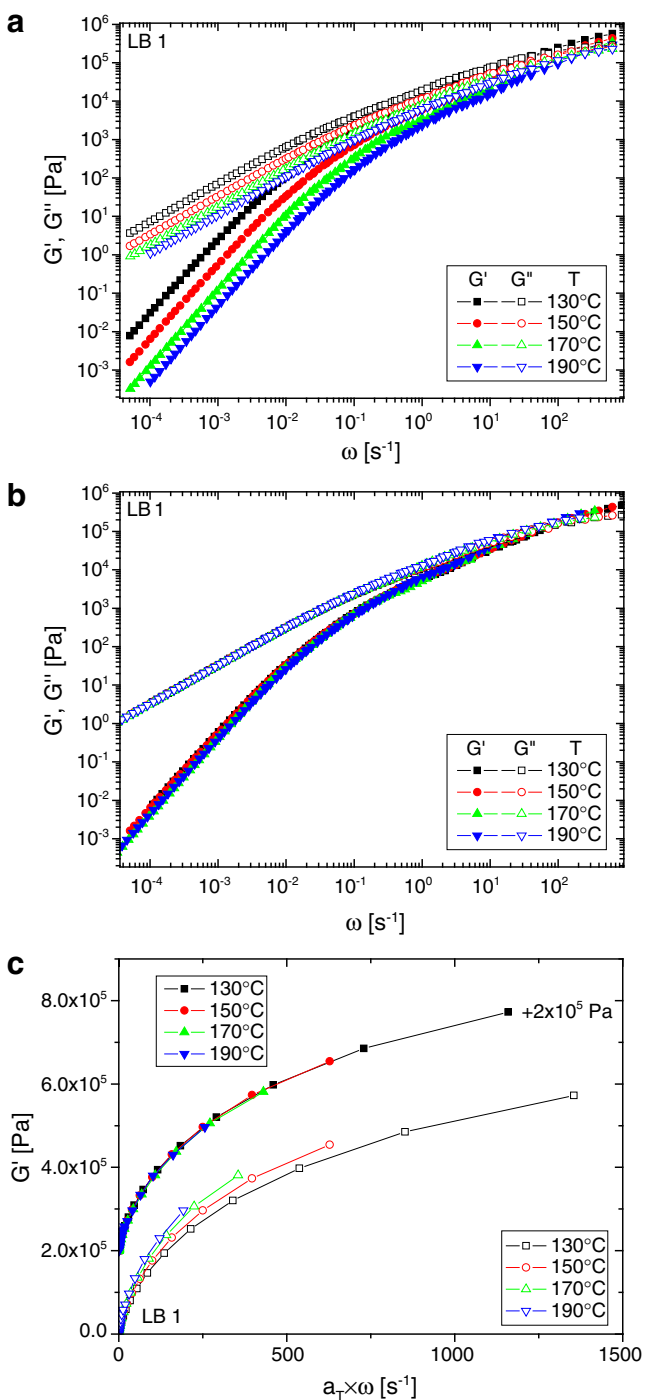


Fig. 2 Complex moduli functions $G'(\omega)$ and $G''(\omega)$ for LB 1. **a** unshifted, **b** $G'(\omega)$ and $G''(\omega)$ shifted by the best fit around $G'(\omega)$ and $G''(\omega) \approx 10^5$ Pa (around ω_c), **c** linear plot of $G'(\omega)$ (open symbols) shifted by the best fit around $G'(\omega)$ and $G''(\omega) \approx 10^5$ Pa (around ω_c) and shifted by the best fit around $G'(\omega)$ and $G''(\omega) \approx 4 \times 10^5$ Pa (filled symbols and shifted by adding 2×10^5 Pa to $G'(\omega)$)

the complex modulus $|G^*|$ ($\delta(|G^*|)$ -plot), which proved to be very sensitive for the detection of thermorheological complexities and is, thus, also used in our analysis

regularly. However, no information on the activation energy can be obtained from the $\delta(|G^*|)$ plot, because none of the quantities has a time dependent component, i.e., a component with time in the physical unit.

However, this apparent disadvantage is its biggest strength; because of the absence of the need to shift, the question whether the material is thermorheologically simple or complex can be answered without any—potentially error afflicted—data manipulation.

The data from frequency sweeps were used in Fig. 3 for plotting the phase angle δ as a function of the absolute value of the complex modulus $|G^*|$ —the $\delta(|G^*|)$ plot.

In Fig. 3, it is shown that for the linear mLLDPE, the curves measured at different temperatures merge on one single curve indicating thermorheological simplicity. For LB 1, the $\delta(|G^*|)$ plots differ significantly from the linear samples, and also for all temperatures,

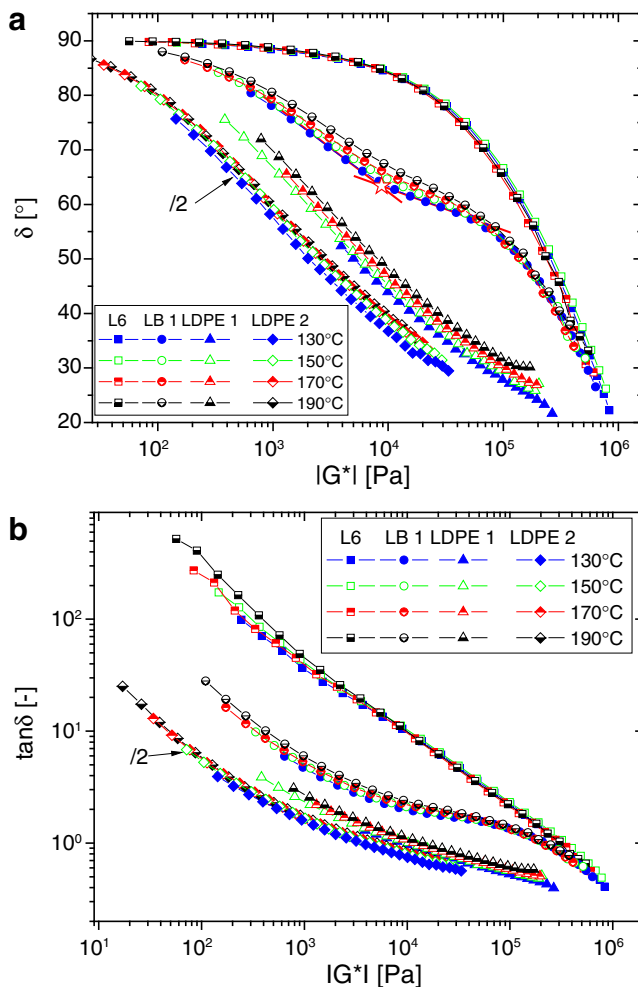


Fig. 3 $\delta(|G^*|)$ plots and $\tan \delta(|G^*|)$ plots measured at different temperatures **a** $\delta(|G^*|)$ plots of L6, LB 1, LDPE 1, and LDPE 2, **b** $\tan \delta(|G^*|)$ plots of L6, LB 1, LDPE 1, and LDPE 2

the shape is different. This is a strong evidence for long-chain branching and thermorheological complexity. Figure 3a also shows the $\delta(|G^*|)$ plots for LDPE 1. The curves of the LDPE are similar in shape, but they do not merge onto one single curve. Instead they are shifted along the $|G^*|$ axis (Keßner et al. 2009). This indicates another type of thermorheological complexity than the one found for LCB-mPE. A similar behavior for LDPE was found by Mavridis and Shroff (1992).

Figure 3a shows the data of both LDPE 1 and 2 (for the sake of distinguishability, the $|G^*|$ data of LDPE 2 was divided by 2), which are very similar in their characteristics despite a factor of ≈ 8 in their η_0 and a very high difference in molar mass M_w as well. The similarity of the rheological data in linear viscoelastic shear is a general property of LDPEs (Stadler et al. 2009).

Based on Fig. 3a, *three different types of thermorheological behavior* can be observed for normal polyethylenes. The linear PEs are thermorheologically simple, i.e., a master curve can be created without any problems by shifting the data along the time or frequency axis. In the $\delta(|G^*|)$ plot, this behavior is obvious as an overlap of the curves at all temperatures within the experimental accuracy.

The LDPEs show approximately the same shape in their viscoelastic functions, best observable in $\delta(|G^*|)$, but shifted along the modulus axis. An increase of the temperature leads to an increase of the modulus, which can be observed as a shift to the right in Fig. 3.

The most complex thermorheological complexity pattern is found for the LCB-mPE. These samples show an agreement of $\delta(|G^*|)$ at high moduli. As soon as $\delta(|G^*|)$ deviates significantly from the linear LLDPE (for PE, this is typically the case around $|G^*| = 200,000$ Pa), the shape of the viscoelastic functions are distinctly different. In all cases reported (Stadler et al. 2008, 2010; Wood-Adams and Costeux 2001), δ reaches a lower minimum or shoulder when decreasing the temperature.

Figure 3b shows the same data plotted as $\tan\delta(|G^*|)$. The data in these plots show the thermorheological complexity of LDPEs and LCB-mPEs in a slightly different manner. The data of LCB-mPE do not converge at low $|G^*|$ like in the $\delta(|G^*|)$ plot, which is the consequence of $\tan\delta$ showing small differences at high δ better than δ itself. Instead they run in an almost perfectly parallel fashion for $|G^*| < 30,000$ Pa.

This difference in δ vs. $\tan\delta$ is also the reason why the mLLDPEs apparently are thermorheologically complex, which, however, is due to experimental inaccuracy as can be seen from the fact that the deviations at high $\tan\delta$ are not systematic. The reason for these deviations lies in the fact that the apparent thermorheological

complexity corresponds to experimental errors around $\pm 0.2^\circ$, which are largely enhanced due to δ being close to 90° .

The differences between the $\delta(|G^*|)$ and the $\tan\delta(|G^*|)$ plots for LDPEs are minimal, as the significant effects occur at $\delta < 45^\circ$, where the difference in the shape due to the tangent function is rather small.

Trinkle et al. (2002) defined the characteristic point p_c in the $\delta(|G^*|)$ plot as the intercept between the tangents laid through the tangents on both sides of the additional curvature of $\delta(|G^*|)$. Figure 3a shows this definition for LB 1 measured at 130°C , where the ψ -symbol marks p_c .

G_c —the x -coordinate of p_c —mainly depends on the molar mass of the different sections of the branched molecules (e.g., the backbone and the long-chain branch length) (Stadler and Karimkhani 2011).

For the further analysis of the rheological data especially of long-chain branched samples, the critical phase angle δ_c , the y -coordinate of p_c , is widely used as an indicator of the level of long-chain branching. Recently, a correlation between δ_c and a characteristic number of long-chain branches per molecules was established for LCB-mPE (Stadler and Karimkhani 2011). δ_c will be intensively discussed later in this paper.

Besides these plots, also a Cole–Cole-plot ($G'(G'')$; Cole and Cole 1941) would be possible for the detection of the thermorheological complexity (Fig. 4). However, due to the large range of $G'(\omega)$ and $G''(\omega)$, the differences are small (the deviations are in the same range as the deviations for the apparent master curves (Fig. 2b)); thus, the plot is not very sensitive. For this reason, the use of this plot for the detection of thermorheological complexity is not recommended.

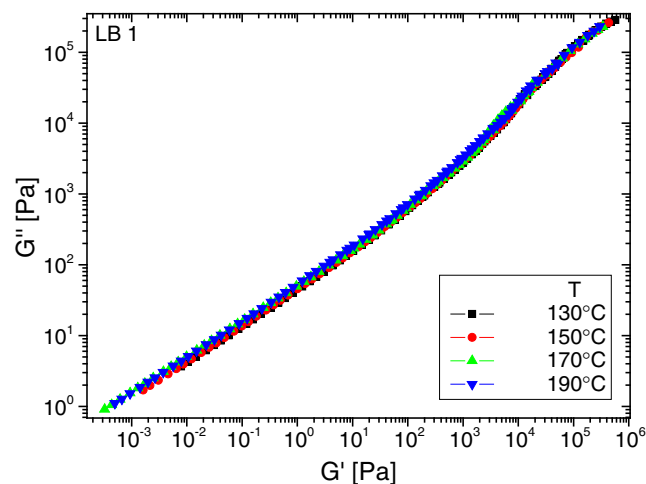


Fig. 4 Cole–Cole plot of LB 1

How can the thermorheological complexity be analyzed?

Basically, there are two ways to do this.

1. The thermorheological complexity is analyzed as a deviation in a plot of a rheological quantity as a function of another quantity, which might be normalized. The best plots for this purpose are the $\delta(|G^*|)$ plots aka van Gorp–Palmen plots (van Gorp and Palmen 1998). Cole–Cole plots in comparison are significantly less sensitive and, therefore, not recommended (Cole and Cole 1941).
2. The analysis is carried out via a piece-wise time-temperature superposition. This means finding the shift factors for a constant value of the shifted quantity ($G'(\omega), G(t), H(\tau), \dots$).

These two methods will be compared in the following.

Deviation method

This method consists of finding the degree of deviation between data at two temperatures for a given x -value, e.g., the magnitude of the complex modulus $|G^*|$. In Fig. 5, the deviation in δ in the $\delta(|G^*|)$ plot at $|G^*| = 10,000$ Pa is used, which shows that the deviation is roughly linear as a function of temperature yielding a difference in δ of 3.7° between 130°C and 190°C . When performing the same analysis at $|G^*| = 1,000$ Pa, the difference is only 2.6° .

This clearly shows that there is a significant problem about this method. The deviation depends on the two

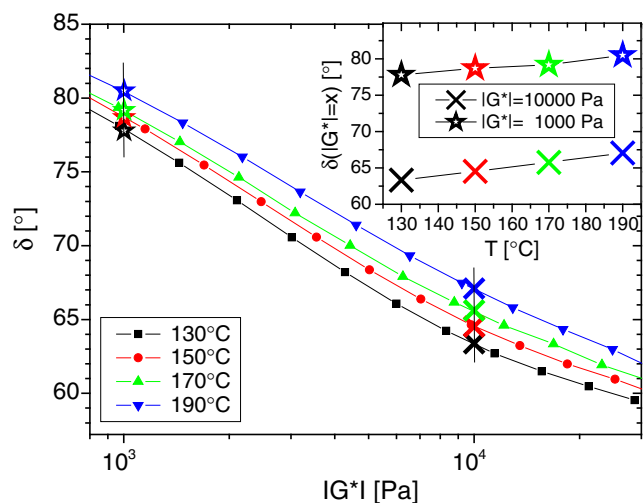


Fig. 5 $\delta(|G^*|)$ plots measured at different temperatures for LB 1

temperatures and on the position (e.g. $|G^*|$) taken for comparison.

When taking another plot, e.g., a pseudo-master curve of $G'(\omega)$, the additional complication is that $a_T(T;T_0)$ has to be chosen for the best fit at an arbitrary point, which means that the result depends on yet another variable, the modulus G' , at which $a_T(T;T_0)$ was chosen to make the best fit. When using a global minimization of $G'(a_T \times \omega)$, roughly the same result will be the case, only that no G' can be defined, at which $a_T(T;T_0)$ was taken but an average, measurement interval dependent value. Hence, using the deviation method for plots involving a time-shift factor ($a_T(T;T_0)$) is scientifically unsound.

In summary, it is concluded that the deviation method can give some qualitative insight. In general, it is useful to state that in the temperature range measured a maximum deviation of x° in δ is found (determined from the $\delta(|G^*|)$ plot). Typically a systematic deviation of at least 1° has to be found to call a material thermorheologically complex.

Piecewise time-temperature superposition method

The basic principle of the piecewise time-temperature superposition method is to not globally find shift factors but to find angular frequencies ω , relaxation times τ , or measurement times t , at which a constant value of the modulus ($G'(\omega), G''(\omega), G(t)$),¹ phase angle ($\delta(\omega)$) or relaxation/retardation strength ($g(\tau), H(\tau)$) (Fig. 6b), $L(\tau)$) is obtained. This principle was first described by Carella et al. (1986) for hPBd, for LDPE and HDPE by Laun (1987), and for mPE by Wood-Adams and Costeux (2001).

Figure 6a shows the relaxation spectra of L6-2, an mLLDPE without long-chain branches, while Fig. 6b shows the same plot for LB 4, an LCB-mLLDPE. It is obvious at a first glance that the relaxation spectra of the linear mLLDPE L6-2 (Fig. 6a) look very much alike, which is a good indicator of thermorheological simplicity, while the spectra of the LCB-mLLDPE LB 4 (Fig. 6b) clearly diverge with increasing relaxation time τ , which means that this sample is thermorheologically complex.

Figure 6c shows the relaxation spectra of LDPE 1, which are very similar in shape, but they do not agree to each other when shifting them onto each other. The

¹Although it has not been attempted to our knowledge also the complex compliance functions ($J'(\omega), J''(\omega)$) or the relaxation modulus $G(t)$ should lead to the same result. Resch et al. (2009) showed that the thermorheological complexity also exists for $J(t)$ and $J_r(t)$.

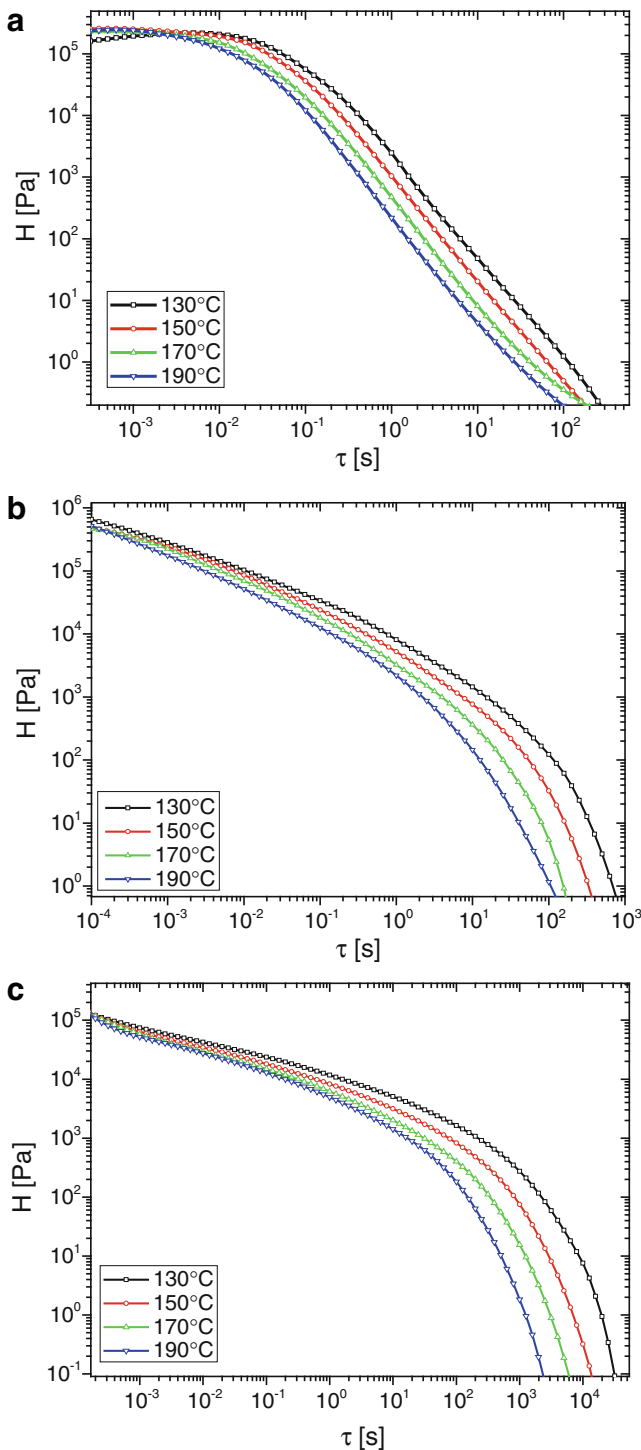


Fig. 6 Relaxation spectra of **a** mLLDPE L6-2, **b** LCB-mLLDPE LB 4, and **c** LDPE 1

offset was previously discussed by Keßner et al. (2009) and is given in a different form in Fig. 3.

Figure 7 gives the storage moduli of B13P, a metallocene catalyzed long-chain branched ethene–propene

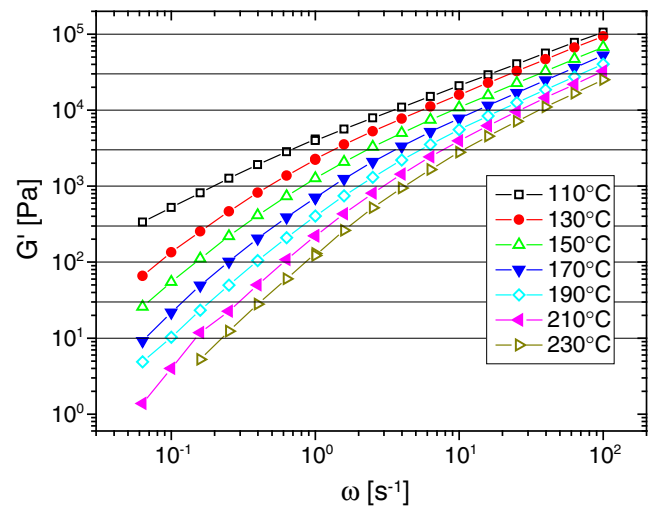


Fig. 7 Plot of the storage modulus $G'(\omega)$ of B13P

copolymer (LCB-mLLDPE). It is obvious that the shape of $G'(\omega)$ changes as a function of temperature; hence, the shift at high $G'(\omega)$ is lower than at low $G'(\omega)$.

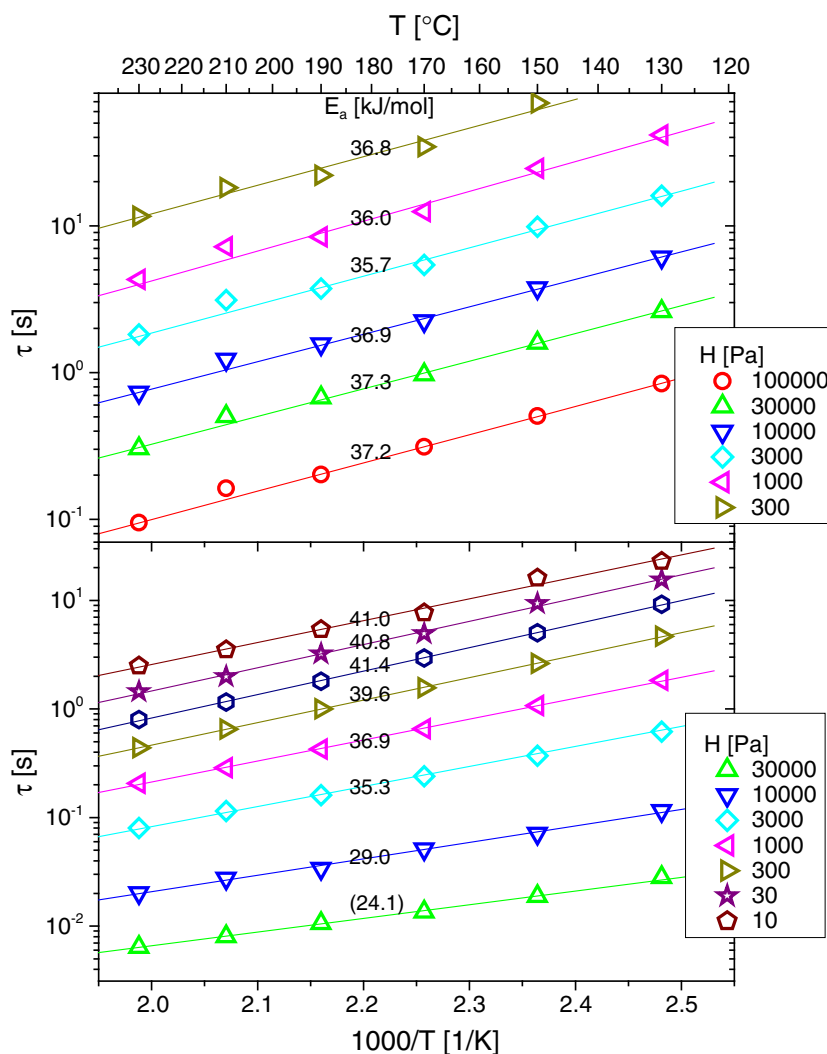
The differences become even more obvious when comparing the Arrhenius plots of a thermorheologically simple material (in this case mLLDPE F18F) and a thermorheologically complex sample, such as LCB-mLLDPE B13P (Fig. 8), calculated from the spectrum. The shift factors determined at different relaxation strengths of F18F show the same slope—and, thus, the same activation energy (Fig. 8 top)—while a decrease of the relaxation strength in B13P leads to a higher slope (Fig. 8 bottom).

The activation energy E_a of F18F of approximately 37 kJ/mol is very high for a PE without long-chain branches. Stadler et al. (2007) established that the activation energy E_a of mLLDPEs scales linearly with the side-chain content. Although F18F does not have a very high molar level of short-chain branching, the high length of the short-chain branches (C18) leads to a very high side-chain content, for which the $E_a \approx 37$ kJ/mol is exactly the expected value.

However, not all rheological quantities react identically to thermorheological complexity. While it is obvious that the scaling of δ on one hand and the moduli and spectra on the other hand are different due to their different physical units, pronounced differences are found when comparing different rheological quantities.

For B13P, for example, the following activation energies were determined $E_a (G' = 300 \text{ Pa}) = 38.3 \text{ kJ/mol}$, $E_a (G'' = 300 \text{ Pa}) = 33.4 \text{ kJ/mol}$, and $E_a (H = 300 \text{ Pa}) = 39.5 \text{ kJ/mol}$. For the frequencies,

Fig. 8 Arrhenius plots of F18F (*top*) B13P (*bottom*) at different values of $g(\tau)$



at which $G' = 300$ Pa, the activation energy determined from δ (at $\approx 77^\circ$) is around 50 kJ/mol.²

For this reason, it is always important to not only say that the activation energy was determined at a certain point, but also which variable was used for this purpose.

When plotting the activation energies determined at different values of G' , G'' , $|G^*|$, δ , and H as a function of that quantity, this becomes even more obvious, as significant differences are found (e.g. shown for LDPE 3 in Fig. 9). In general, at high G' , G'' , $|G^*|$, and H a lower

activation energy is found, which then approaches a saturation value in the terminal regime (low G' , G'' , $|G^*|$, and H). As Keßner et al. (2009) reported, for LDPE, $E_a(\delta)$ is roughly constant. However, as will be shown later, this is not true for LCB-mPE. The dependence of $E_a(\delta)$ on the molecular architecture is discussed in detail by Keßner and Münstedt (2010).

Why are the activation energy spectra different for different for different rheological quantities?

Figure 9 clearly demonstrates that the activation energy spectrum depends on the rheological quantity used for its determination.

This raises the question, as to why evaluating $G'(\omega)$, $G''(\omega)$, $|G^*|(\omega)$, and $H(\tau)$ piecewise for the determination of the activation energy spectrum lead to different values.

²The activation energy E_a determined from δ cannot be stated exactly, as the value of 300 Pa occurs at different angular frequencies for $G'(\omega)$, $G''(\omega)$ and $H(\tau)$. The value given represents an average of the activation energy around the frequency at which $G'(\omega) = 300$ Pa and $H(\tau) = 300$ Pa.

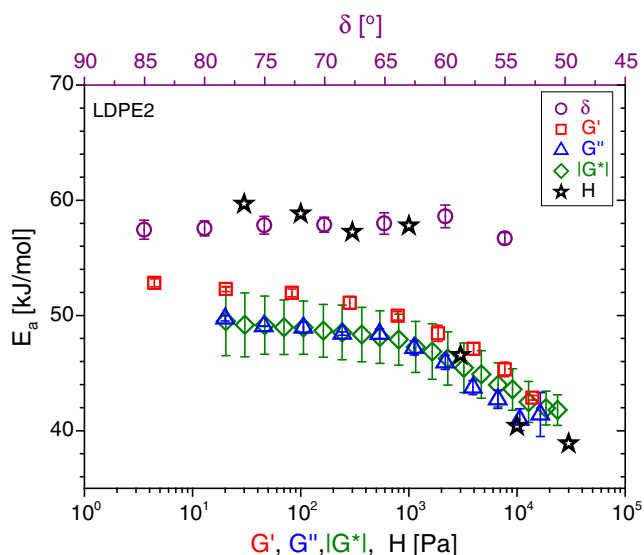


Fig. 9 Activation energy E_a determined by piecewise time-temperature superposition as a function of the values, for which these were determined (G' , G'' , $|G^*|$, δ , and H). Data partially adapted from Keßner (2010)

To explain this visually, the relevance factors defined by one of us earlier (Stadler 2010) are discussed. The relevance factors $r'(\omega, \tau)$ and $r''(\omega, \tau)$ are the fingerprint of the spectrum and show which relaxation time τ contributes to which extent to the G' or G'' at a given frequency ω , respectively. It was found that the most convenient representation of these data is a contour plot, where a higher importance of a certain τ for a certain ω is represented by a darker gray.

Figure 10 shows the relevance factor plots with the activation energies for $H(\tau)$, $G'(\omega)$, and $G''(\omega)$ added as numbers with vertical and horizontal lines, respectively. It is obvious from this representation that the activation energy of the spectrum at the most relevant (=darkest) region along a green, horizontal line determines the activation energy most, although also the less relevant relaxation modes contribute.³

It is clear from a comparison of Fig. 10a and b that $G'(\omega)$ depends primarily on much longer relaxation modes than $G''(\omega)$. As the longer relaxation modes have a higher activation energy, $G'(\omega)$ —consequently—also has a higher activation energy than $G''(\omega)$, which explains the finding of Fig. 9 of $G''(\omega)$ having a lower E_a than $G'(\omega)$.

The similarity of $E_a(G'')$ and $E_a(|G^*|)$ is easily explained by the fact that at high moduli (\geq high ω) the

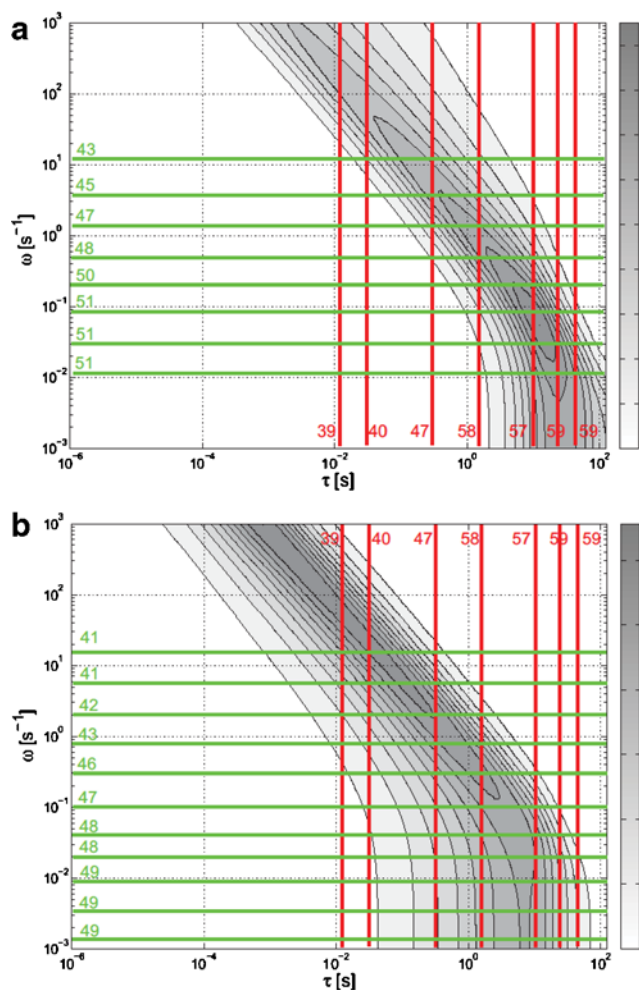


Fig. 10 Relevance factor plot for LDPE 2 at 150°C. The red numbers with vertical lines stand for the activation energies E_a determined from H , the green numbers with the horizontal lines stand for the activation energies E_a [kJ/mol] determined from G' (a) G'' (b), respectively. **a** $r'(\omega, \tau)$, **b** $r''(\omega, \tau)$

activation energies for $G'(\omega)$ and $G''(\omega)$ as well as for $H(\tau)$ are almost identical. At low frequencies (low $|G^*|(\omega)$), $G'(\omega)$ is much smaller than $G''(\omega)$; hence, the latter dominates $|G^*|(\omega)$ and, therefore, also $E_a(|G^*|)$. The same behavior is also expected for $E_a(|\eta^*|)$.

Deciding which variable is the best to determine the activation energy is not obvious, however, the relaxation spectrum (or the retardation spectrum) offers the best chances to get an insight into the molecular mechanisms.

The reason for that is that the relaxation spectrum $H(\tau)$ is the material function, from which all other rheological quantities can be derived. This method will, therefore, lead to structure relevant activation energies. This method was proposed by Wood-Adams and Costeux (2001) and Stadler et al. (2008).

³Please note that the lines are not equidistant as they were determined at constant relaxation strength or modulus, while Fig. 10 plots frequency and relaxation time.

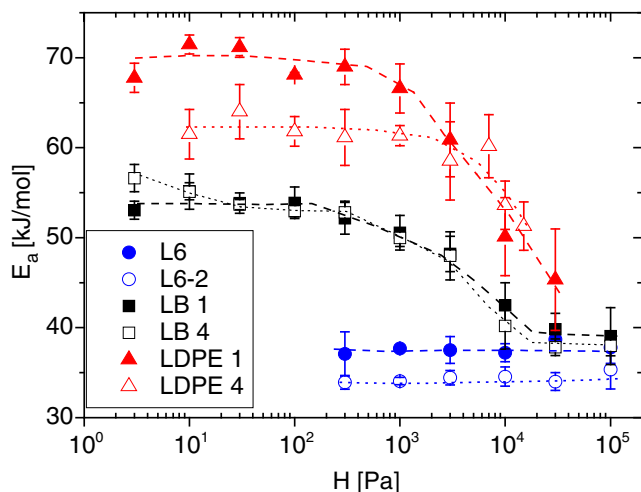


Fig. 11 Activation energies E_a determined from relaxation spectra for different relaxation strength H . No modulus shift factor b_T was taken to determine E_a

Thermorheological behavior and its relation to the molecular structure

For all characteristic relaxation times, an Arrhenius equation holds for describing the temperature dependencies. Figure 11 shows the activation energies E_a as a function of relaxation strength H . When determining the shift factors from “iso relaxation strength slices”, self-evidently, a modulus/relaxation strength shift (b_T) to improve the quality of the “master spectrum” is not possible. In this way, the methods of modulus shifting (Keßner et al. 2009) and of determining the activation energy spectrum (Stadler et al. 2008) compete with each other.

The linear mLLDPE show constant activation energies, as the shape of the spectra is the same for all temperatures. This explains the thermorheologically simple behavior and thus the independence of temperature for J_e^0 . The activation energies of L6 and L6-2 are 37.7 and 34.6 kJ/mol, respectively. This is in agreement with literature (Kim et al. 1996; Stadler et al. 2007; Wood-Adams 1998).

For the LCB-mLLDPE, the activation energies increase with decreasing relaxation strength from approximately 40 to 54 kJ/mol for LB 1 and to 57 kJ/mol for LB 4. Within the measured temperature regime, different shift-factors have to be applied for different regimes of the spectrum and the materials behave thermorheologically complex.

The LDPE has constant activation energies in the terminal regime at low relaxation strengths where the spectra have the same shape. In this regime, the materials behave thermorheologically simple and J_e^0 is

independent of temperature. But for high relaxation strengths, a decrease in activation energy is found that indicates a thermorheological complexity in the rubbery plateau. For LDPE 1, this behavior is more pronounced than for LDPE 4. A terminal activation energy of 62 kJ/mol was determined for LDPE 1 and of 70 kJ/mol for LDPE 4.

Difference in the thermorheological complexity of LCB-mPE and LDPE

Based on above results, especially concerning the activation energy spectrum, one might argue that there is no difference in the thermorheological complexity of LCB-mPE and LDPE; however, this apparent finding only holds as long as the activation energy is determined from the spectrum or the modulus functions.

However, as Keßner et al. (2009) demonstrated, the thermorheological complexity can be eliminated when introducing a modulus shift factor b_T . To demonstrate this in the spectra, the ratio of the relaxation spectrum at $T = 150^\circ\text{C}$ and 190°C , was shifted to $T_0 = 150^\circ\text{C}$ using the shift factors a_T determined from $\delta(\omega)$. In case of LB 1, $E_a = 40$ kJ/mol was taken, which is the activation energy around ω_c . Figure 12 shows that the shape of the spectrum is approximately constant for the LLDPE L6-2 and LDPE 1. However, unlike for the LLDPE the ratio between the two temperatures for the LDPE is not 1 but approximately 1.4. In other words, the LDPE-spectra can be used to create a master spectrum, if a proper shift factor b_T is used.

This is the same shift factor b_T , which Keßner et al. (2009) defined via the ratios of the steady-state elastic recovery compliances $J_e^0(T)$. Thus, evidence is supplied

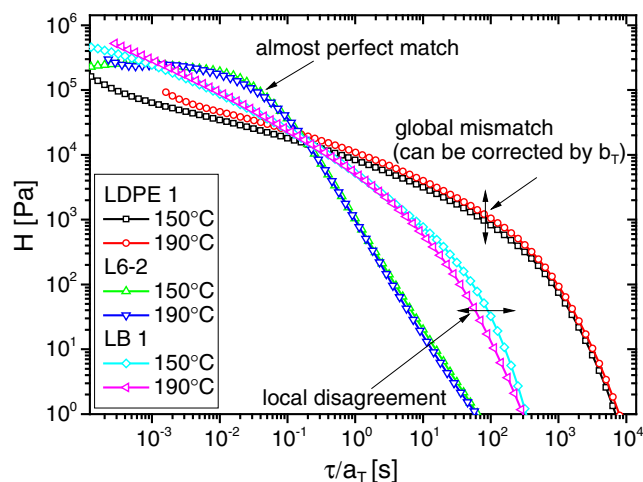


Fig. 12 Comparison of shifted spectra of LDPE 1, L6-2, and LB 1

that the modulus/compliance/relaxation strength shift concept of Keßner et al. (2009) (which was originally postulated by Mavridis and Shroff (1992) in a different fashion) is correct for LDPEs.

The shape of the LCB-mPE LB 1-spectrum, however, shows that neither $b_T = 1$ (thermorheological simplicity) nor a constant b_T (LDPE-type thermorheological complexity) will lead to an acceptable master spectrum. At short relaxation times, the 190°C spectrum is located at higher relaxation times than of the 150°C spectrum, although the 190°C spectrum is shifted. At long relaxation times, the 150°C spectrum is located at higher relaxation times than the 190°C spectrum.

From the relaxation spectrum, the steady-state elastic recovery compliance J_e^0 is defined as

$$J_e^0 = \frac{\int_0^{\infty} H(\tau) \cdot \tau^2 d \ln \tau}{\left(\int_0^{\infty} H(\tau) \cdot \tau d \ln \tau \right)^2} \quad (\text{Ferry 1980}). \quad (3)$$

For including temperature dependence into this equation, the “time” shift factor a_T and the “modulus” shift factor b_T have to be introduced into Eq. 3 as

$$\begin{aligned} J_e^0 &= \frac{\int_0^{\infty} b_T H(a_T \tau) \cdot (a_T \tau)^2 d \ln \tau}{\left(\int_0^{\infty} b_T H(a_T \tau) \cdot a_T \tau d \ln \tau \right)^2} \\ &= \frac{a_T^2 b_T}{a_T^2 b_T^2} \frac{\int_0^{\infty} H(\tau) \cdot \tau^2 d \ln \tau}{\left(\int_0^{\infty} H(\tau) \cdot \tau d \ln \tau \right)^2} \\ &= \frac{1}{b_T} \frac{\int_0^{\infty} H(\tau) \cdot \tau^2 d \ln \tau}{\left(\int_0^{\infty} H(\tau) \cdot \tau d \ln \tau \right)^2}. \end{aligned} \quad (4)$$

This simplification is only possible because a_T and b_T are defined as constants. Hence, they can be extracted from the integral and the fractions can be reduced. The direct effect of this is that a global b_T can be deduced from the ratio of the values of J_e^0 at different temperatures, which is exactly what Keßner et al. (2009) found using a different approach.

Alternatively, also other definitions for the “modulus” shift factor b_T would be possible, such as the modulus at the crossover frequency ω_c . Such a definition

would lead to the same b_T within the experimental accuracy.⁴

Discussion

Possible explanations for the modulus shift of LDPE

The question is why LDPE has such temperature dependence involving a modulus shift. An effect, which could cause that behavior, is an effect related to the geometry of the rheometer such as an imperfect compensation of the thermal expansion or temperature dependent plate adhesion. Careful experiments (e.g. by Keßner et al. 2009) and also the common sense safely rule out this possibility.

Keßner et al. (2009) convincingly demonstrated that a possible density change would have to be so unusually large that it cannot be responsible for this type of behavior. All facts discussed by Keßner et al. (2009) and here, however, clearly show that the vertical shift applies to the whole measured curve including the plateau modulus G_N^0 .

This implies another explanation: As G_N^0 and the entanglement molar mass M_e are closely linked to each other, a strong temperature dependence of M_e could be made responsible for the modulus shift as well. Such a change in M_e , however, would not only shift G_N^0 but also the number of entanglements on a chain. As LDPE is long-chain branched, this would mean that some unentangled side chains would suddenly behave as entangled ones when increasing the temperature. Such an effect would certainly change G_N^0 in the desired fashion but would also lead to the lengthening of the terminal relaxation time and, thus, would lead to an LCB-mPE-type thermorheological complexity, which clearly is not the case. Furthermore, it would also lead to a temperature dependence of the strain hardening, while this quantity was found to be temperature independent (Stadler et al. 2009).

Another possibility for explaining the anomalous temperature dependence of LDPE could be found when reminding that, typically, the short-chain branch (SCB) content increases with growing molar mass M (Shirayama et al. 1965). PE with different SCB contents, however, are only partially miscible so that we, a priori, have to understand LDPE as a partially phase

⁴Equation 4 also allows for a very simple proof that J_e^0 is temperature independent for linear PE (e.g. LLDPE). One simply has to assume that b_T is equal to unity over the whole temperature range. Then J_e^0 is independent of temperature, no matter how large a_T is.

separated system. Additionally, it has to be considered that LDPE also has a large gradient in LCB content, which further fosters the phase separation. As such a phase separation is driven by enthalpy and entropy, it must have a temperature dependence. A mechanical strain cannot be transported across a phase boundary easily, because the phase boundary is much weaker than the bulk material. A temperature dependence of this phase separation process would change the strength of the phase boundary and, thus, lead to a modulus shift *without* changing the spectrum in a measurable way in its shape.

A closely related effect could also be that the low molecular oligomers, which make up a sizable portion of LDPE (after all M_n of a typical LDPE is in the order of 10 kg/mol), could tend to phase separate more at low temperatures and, thus, form low molecular slip layers, which are responsible for the lower moduli at low T .

This effect could be related to the refining effect of highly branched polymer melts (mostly LDPEs) reported previously (Breuer and Schausberger 2011; Münstedt 1981; Rokudai and Fujiki 1981; Stange et al. 2005). The refining effect is the change of the rheological properties by applying a strong mechanical deformation in a physical way. The proof of the physical (and not chemical) nature of this effect was conducted by dissolving the extruded material, which returns the original properties. One explanation was that the entanglement structure is changed. However, besides that, also a possible partially phase separated structure will be strongly affected by an intensive mechanical treatment.

Although the partial phase separation and the related refining effect are very plausible explanations for the effect, they cannot be proven with any method known to the authors.

Thermorheological complexity in LCB-mPE and temperature dependence of J_e^0

Thermorheological complexity in LCB-mPE and the temperature dependence of J_e^0 become logical when taking the correlation between the ratio of the real zero shear-rate viscosity to the zero shear-rate viscosity expected from molar mass $\eta_0/\eta_0^{\text{lin}}$ and the critical phase angle δ_c into account (Stadler and Karimkhani 2011).

It was already postulated by Stadler et al. (2008) that a relaxation spectrum of an LCB-mPE can be deconvoluted in a linear and a long-chain branched part of the spectrum. The linear part is faster and has higher relaxation strengths, while the long-chain branched one is very slow and has lower relaxation strength. Therefore, LCB-mPE can be considered to be

a blend of linear and long-chain branched chains with the long-chain branched fraction being predominantly made up of star-like chains. Depending on the degree of long-chain branching, the ratio of the two fractions vary; typically, 50% or more of the chains are linear. For an LCB-mHDPE with $M_w = 100$ kg/mol and $M_n = 50$ kg/mol, an average degree of long-chain branching $\lambda = 2.8$ LCB/10,000 Monomer has to be present in order to have 0.5 long-chain branches per molecule.⁵

Münstedt et al. (2006) clearly showed the connection between long-chain branching and processing behavior in elongation dominated operations (film blowing, blow molding, ...). Gabriel and Münstedt (2003), however, showed that while the low degree of long-chain branching has a significant influence on the shear rheological behavior, the strain hardening levels of LCB-mPE are significantly below the levels found for LDPEs, which means that their processing behavior is somewhat better than for normal mLLDPE or (Ziegler-Natta) ZN-LLDPE, but that the very good processing behavior in such elongation dominated processing properties is still significantly worse than that of classical LDPEs.

The different branching topography of LCB-mPE and LDPE also leads to differences in the strain rate dependence of the strain hardening. LDPE has a very high level of strain hardening at high strain rates, while LCB-mPE is predominantly strain hardening at low strain rates, close to the Newtonian regime. This difference makes LDPEs more suitable for processes where fast elongational deformations occur, e.g. film blowing, foaming, or fiber spinning, while LCB-mPE are more suitable for preventing sagging due to gravity and slow extensions, occurring for example in blow molding (Münstedt et al. 2006). This difference can be explained by the spectrum of LB 1 (Fig. 13), which shows that the long-chain branched molecules are mainly visible at longer relaxation times for LCB-mPE and, therefore, can only lead to strain hardening at slower elongation rates. For LDPE, the content of linear chains is very small and the linear chains existing are predominantly very low molecular (Tackx and Tackx 1998). Hence, long-chain branched chains dominate the experimental range accessible by rheology.

Figure 13 shows the linear reference spectrum (Stadler and Mahmoudi 2011a) in comparison to the

⁵This would correspond to a linear fraction of 50%, when assuming that this LCB-mHDPE is only a mixture of linear chains and 3-arm stars. However, in reality there will be also higher branched chains, which means that the linear fraction is larger than 50%. This degree of long-chain branching is typical for LCB-mPE with molar masses around $M_w = 100$ kg/mol (Stadler and Karimkhani 2011).

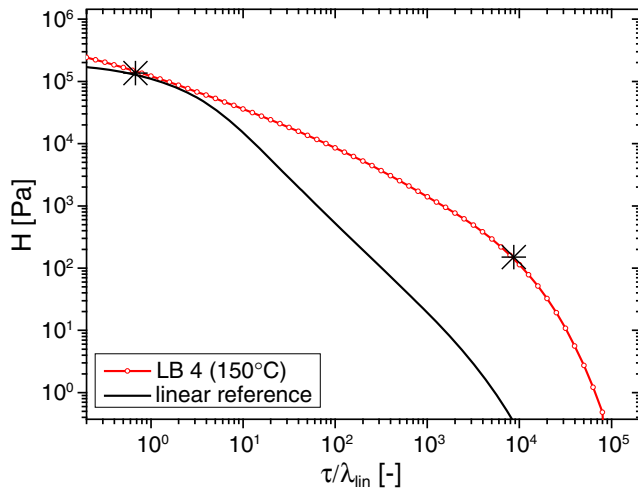


Fig. 13 Relaxation spectrum of LB 4 and the linear reference normalized to the characteristic relaxation time

spectrum of LB 4 at 150°C. To correct for the molar mass, the spectra were normalized to the characteristic relaxation time λ_{lin} determined from the molar mass M_w according to the scaling law

$$\lambda_{lin} = 8.4 \cdot 10^{21} \cdot M_w^{3.6}, \tag{5}$$

established for linear and short-chain branched polyethylenes before (Stadler and Münstedt 2008a; Stadler et al. 2006), which is slightly comonomer content dependent (Stadler and Mahmoudi 2011b).

For LDPE, such a separation into a linear and a long-chain branched part of the spectrum cannot be performed, as LDPE lacks a significantly entangled linear fraction, which could be taken as linear reference.

Because of the separability of linear and long-chain branched part of the spectrum, it is possible to simplify the spectrum into a 2-mode spectrum, e.g., by using two modes indicated by the asterisks in Fig. 13. g_{lin} and g_{lcb} stand for the relaxation strength of the linear and the long-chain branched mode, respectively, τ_{lin} and τ_{lcb} for the corresponding relaxation times. This simplification—although undoubtedly error afflicted (this was previously discussed in the last section of Resch et al. (2011)—running integrals)—means that the problem can be handled easily in an analytical manner. Equation 3 can, therefore, be simplified into

$$J_e^0 = \frac{g_{lin} \cdot \tau_{lin} + g_{lcb} \cdot \tau_{lcb}^2}{(g_{lin} \cdot \tau_{lin} + g_{lcb} \cdot \tau_{lcb})^2}. \tag{6}$$

The temperature dependence can be introduced as

$$J_e^0 = \frac{g_{lin} \cdot (a_{T_{lin}} + \tau_{lin})^2 + g_{lcb} \cdot (a_{T_{lcb}} \cdot \tau_{lcb})^2}{(g_{lin} \cdot a_{T_{lin}} \cdot \tau_{lin} + g_{lcb} \cdot a_{T_{lcb}} \cdot \tau_{lcb})^2}, \tag{7}$$

Where $a_{T_{lin}}$ and $a_{T_{lcb}}$ stand for the shift factors of the linear and long-chain branched mode. In order to simplify this further, the contribution of $a_{T_{lcb}}$ is separated into $a_{T_{lin}}$ and $a_{T_{lcb}}$ as

$$a_{T_{lcb}} = \frac{a_{T_{lcb}'}}{a_{T_{lin}}}, \tag{8}$$

which leads to

$$\begin{aligned} J_e^0 &= \frac{a_{T_{lin}}^2 \cdot g_{lin} \cdot \left(\frac{a_{T_{lin}}}{a_{T_{lin}}} \cdot \tau_{lin}\right)^2 + g_{lcb} \cdot \left(\frac{a_{T_{lcb}'}}{a_{T_{lin}}} \cdot \tau_{lcb}\right)^2}{a_{T_{lin}}^2 \cdot \left(g_{lin} \cdot \frac{a_{T_{lin}}}{a_{T_{lin}}} \cdot \tau_{lin} + g_{lcb} \cdot \frac{a_{T_{lcb}'}}{a_{T_{lin}}} \cdot \tau_{lcb}\right)^2} \\ &= \frac{g_{lin} \cdot \tau_{lin}^2 + g_{lin} (a_{T_{lcb}} \cdot \tau_{lcb})^2}{(g_{lin} \cdot \tau_{lin} + g_{lcb} \cdot a_{T_{lcb}} \cdot \tau_{lcb})^2}. \end{aligned} \tag{9}$$

This simplification can be done as J_e^0 does not depend on $a_{T_{lin}}$ and $a_{T_{lcb}'}$, but only on their ratio, determining the ratio of τ_{lin} and τ_{lcb} .

The temperature dependence of J_e^0 can then be modeled assuming a given difference in activation energies ΔE_a between the linear and the long-chain branched mode, which is in accordance with Stadler et al. (2008) and also given in Fig. 11. The introduction of ΔE_a leads to $a_{T_{lcb}}(T)$ being defined as

$$a_{T_{lcb}} = \exp\left(2.303 \cdot \frac{\Delta E_a}{R} \left(\frac{1}{T} - \frac{1}{T_0}\right)\right), \tag{10}$$

which leads to the temperature dependence of $J_e^0(T)$ being describable by the equation

$$J_e^0(T) = \frac{g_{lin} \cdot \tau_{lin}^2 + g_{lcb} \cdot \left(\exp\left(2.303 \cdot \frac{\Delta E_a}{R} \left(\frac{1}{T} - \frac{1}{T_0}\right)\right) \cdot \tau_{lcb}\right)^2}{\left(g_{lin} \cdot \tau_{lin} + g_{lcb} \cdot \exp\left(2.303 \cdot \frac{\Delta E_a}{R} \left(\frac{1}{T} - \frac{1}{T_0}\right)\right) \cdot \tau_{lcb}\right)^2}. \tag{11}$$

If we put realistic numbers into that equation (e.g., $g_{lin} = 200,000$ Pa, $\tau_{lin} = 0.01$ s, $g_{lcb} = 1,000$ Pa, and $\tau_{lcb} = 10$ s (at 150°C)), Eq. 11 leads to a temperature dependence of J_e^0 exactly the way described by Resch et al. (2009). Some examples for that are given in Fig. 14, depending on the ratio of τ_{lin}/τ_{lcb} and g_{lin}/g_{lcb} and ΔE_a a more or less pronounced dependence of $J_e^0(T)$ is found as well as realistic values of J_e^0 (Gabriel et al. 2002; Gabriel and Münstedt 2002).

An estimate of the realistic values of τ_{lin} and τ_{lcb} can be obtained from $\lambda_1 (\approx \tau_{lcb})$ and $\lambda_2 (\approx \tau_{lin})$ (Stadler and Münstedt 2008b, c). The ratio of τ_{lin} and τ_{lcb} is approximately independent of the degree of long-chain branching (Stadler and Münstedt 2009), but—self-evidently—depends on the temperature and can thus be obtained

from the molar mass M_w with sufficient accuracy. The correct values of g_{lin} and g_{lcb} can be obtained from the following thoughts. Besides the steady-state elastic recovery compliance J_e^0 , also other viscoelastic quantities can be calculated from the spectrum. The zero shear-rate viscosity η_0 is defined as

$$\eta_0 = \sum_{i=1}^n g_i \cdot \tau_i = \int_0^\infty H(\tau) \cdot \tau d \ln \tau. \quad (12)$$

If we assume that only two modes exist and that one mode is caused by the linear and the other one by the long-chain branched chains, the zero shear-rate viscosity increase factor η_0/η_0^{lin} can be easily calculated as

$$\frac{\eta_0}{\eta_0^{lin}} = \frac{g_{lin} \cdot T_{lin} + g_{lcb} \cdot \tau_{lcb}}{g_{lin} \cdot T_{lin}}. \quad (13)$$

With this knowledge, it should be possible to find an appropriate approximation for the real situation (Fig. 13) as:

$$\frac{\eta_0}{\eta_0^{lin}} = \frac{g_{lin} \cdot \tau_{lin} + g_{lcb} \cdot \left(\exp \left(2.303 \cdot \frac{E_a}{R} \left(\frac{1}{T} - \frac{1}{T_0} \right) \right) \cdot \tau_{lcb} \right)^2}{g_{lin} \cdot \tau_{lin}}. \quad (14)$$

Using the same argument as for $J_e^0(T)$ (Eqs. 6–11), also the zero shear-rate viscosity increase factor has a temperature dependence (Fig. 14). Just like J_e^0 , η_0/η_0^{lin} decreases with rising temperature, because the two main relaxation modes move closer together. The direct result of that is the suggestion that small amounts of long-chain branches should best be detected just above the melting temperature of the material, as the effect of them will be the largest then.

The same effect of the reduction of the efficiency of the long-chain branches with increasing temperature can be also seen in the $\delta(|G^*|)$ plot, which has proven to very sensitively react to small amounts of long-chain branches. Figure 3 shows that the deviation from the linear reference of LCB-mPE decreases with rising T . This is equivalent to an increase of the characteristic phase angle δ_c with increasing T . Because δ_c and η_0/η_0^{lin} are both quantifiers for the amount of long-chain branching in an LCB-mPE, the conclusion is that the efficacy of the LCBs also decreases with increasing T using this quantifier. This becomes evident when knowing that δ_c and η_0/η_0^{lin} are linked by empirical relations through a linear relationship (Stadler and Karimkhani 2011). A high efficacy of long-chain branching leads to an increase in η_0/η_0^{lin} and to a decrease in δ_c .

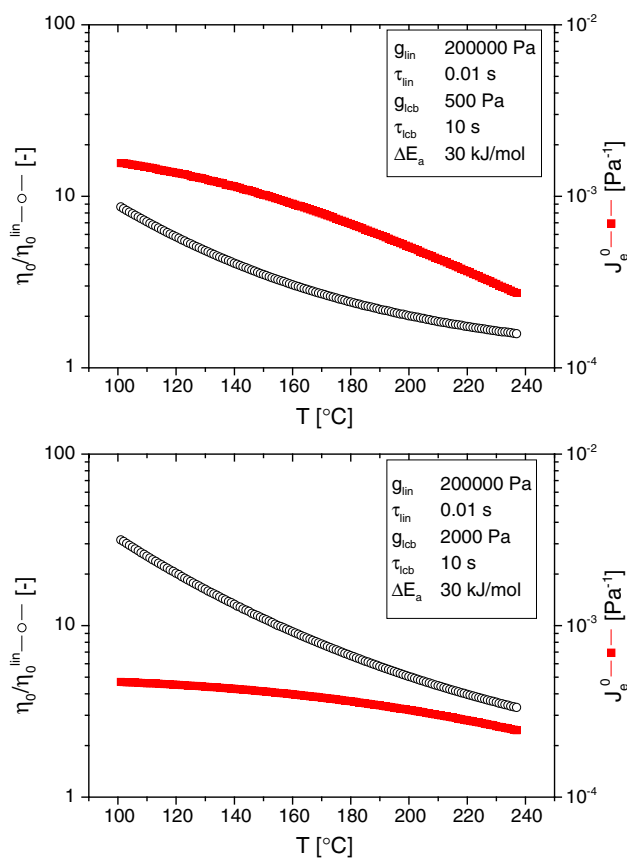


Fig. 14 $J_e^0(T)$ and $\eta_0/\eta_0^{lin}(T)$ for several theoretical bidisperse spectra with $\Delta E_a = 30$ kJ/mol. The exact values put into Eqs. 11 and 14 are denoted in the legend of each subfigure

Summary

The thermorheological behavior of polyethylenes is quite diverse and requires the knowledge of the branching architecture and the temperature dependent physics. Thus, this behavior is far from trivial and has not been explained in detail yet.

The thermorheologically simple HDPEs and LLDPEs are rather easy to understand, while the two different types of thermorheologically complex behavior of LDPE and LCB-mPE make an explanation rather hard.

LDPE shows a thermorheological complexity, which can be compensated for by applying a modulus shift. This modulus shift is stronger than the density compensation. An explanation cannot be given with absolute certainty. However, the most likely reason is a temperature dependence of the miscibility of the different molar mass fractions, which also differ in their SCB content.

LCB-mPEs have a spectrum being essentially made up of contributions of linear and long-chain branched

chains, which have their own distinctly different activation energy E_a . The long modes, dominated by branched chains and thus by a high E_a move closer to the faster modes of the linear chains. This changes the width of the spectrum as well as its shape. Hence, no master curve can be constructed. The consequence of this is also a temperature dependence of δ_c , J_e^0 , and $\eta_0/\eta_0^{\text{lin}}$.

These different types of thermorheological behavior for different molecular architecture open up the possibility of using the temperature dependence of the rheological properties as a probe to the molecular architecture. The currently available data have demonstrated the different types of behavior that are encountered. The authors are certain that more in-depth investigations will lead to a deeper understanding of this relatively unexplored field. However, further discoveries can best be expected from the use of model polymers.

Acknowledgements FJS would like to acknowledge financial support from the “Human Resource Development (Advanced track for Si-based solar cell materials and devices, project number: 201040100660)” of the Korea Institute of Energy Technology Evaluation and Planning (KETEP) grant funded by the Korea government Ministry of Knowledge Economy. JAR gratefully acknowledges the German Research Foundation (DFG) for the financial support of parts of this work.

References

- Arrhenius S (1916) The viscosity of pure liquids. *Meddelanden Från K Vetenskapsakademiens Nobelinstitut* 3:1–40
- Brant P, Canich JAM, Dias AJ, Bamberger RL, Licciardi GF, Henrichs PM (1994) long-chain branched polymers and a process to make long-chain branched polymers. *Int Pat Appl WO 94/07930*
- Breuer G, Schausberger A (2011) The recovery of shear modification of polypropylene melts. *Rheol Acta* (in press)
- Carella JM, Gotro JT, Graessley WW (1986) Thermorheological effects of long-chain branching in entangled polymer melts. *Macromolecules* 19(3):659–667. doi:10.1021/ma00157a031
- Cole KS, Cole RH (1941) Dispersion and absorption in dielectrics - i alternating current characteristics. *J Chem Phys* 9:341–352. doi:10.1063/1.1750906
- Dealy J, Larson RG (2006) Structure and rheology of molten polymers—from structure to flow behavior and back again. Munich, Hanser
- Fawcett EW, Gibson RO, Perrin MW, Paton JG, Williams EG (1937) Ethylene polymers. Imperial Chemical Industries Ltd, Great Britain
- Ferry JD (1980) Viscoelastic properties of polymers. Wiley, New York
- Gabriel C, Münstedt H (2002) Influence of long-chain branches in polyethylenes on linear viscoelastic flow properties in shear. *Rheol Acta* 41(3):232–244
- Gabriel C, Münstedt H (2003) Strain hardening of various polyolefins in uniaxial elongational flow. *J Rheology* 47(3): 619–630
- Gabriel C, Kaschta J, Münstedt H (1998) Influence of molecular structure on rheological properties of polyethylenes I. Creep recovery measurements in shear. *Rheol Acta* 37(1): 7–20. doi:10.1007/s003970050086
- Gabriel C, Kokko E, Löfgren B, Seppälä J, Münstedt H (2002) Analytical and rheological characterization of long-chain branched metallocene-catalyzed ethylene homopolymers. *Polymer* 43(24):6383–6390
- Hepperle J, Münstedt H (2006) Rheological properties of branched polystyrenes: nonlinear shear and extensional behavior. *Rheol Acta* 45(5):717–727
- Hepperle J, Münstedt H, Haug PK, Eisenbach CD (2005) Rheological properties of branched polystyrenes: linear viscoelastic behavior. *Rheol Acta* 45(2):151–163
- Jacovic MS, Pollock D, Porter RS (1979) A rheological study of long branching in polyethylene by blending. *J Appl Polym Sci* 23:517–527
- Kapnistos M, Vlassopoulos D, Roovers J, Leal LG (2005) Linear rheology of architecturally complex macromolecules: comb polymers with linear backbones. *Macromolecules* 38(18):7852–7862. doi:10.1021/ma050644x
- Kaschta J, Schwarzl FR (1994a) Calculation of discrete retardation spectra from creep data: 1. method. *Rheol Acta* 33(6):517–529. doi:10.1007/BF00366336
- Kaschta J, Schwarzl FR (1994b) Calculation of discrete retardation spectra from creep data: 2. analysis of measured creep curves. *Rheol Acta* 33(6):530–541. doi:10.1007/BF00366337
- Kaschta J, Stadler FJ (2009) Avoiding waviness in the calculation of relaxation spectra. *Rheol Acta* 48(6):709–713. doi:10.1007/s00397-009-0370-z
- Keßner U (2010) Thermorheology as a method to investigate the branching structures of polyethylenes. Sierke, Göttingen
- Keßner U, Münstedt H (2010) Thermorheology as a method to analyze long-chain branched polyethylenes. *Polymer* 51(2):507–513
- Keßner U, Kaschta J, Münstedt H (2009) Determination of method-invariant activation energies of long-chain branched low-density polyethylenes. *J Rheol* 53(4):1001–1016. doi:10.1122/1.3124682
- Kim Y-M, Kim C-W, Park J-K, Kim J-W, Min T-A (1996) Short chain branching distribution and thermal behavior of High-density polyethylene. *J Appl Polym Sci* 60:2469–2479
- Lai SY, Wilson JR, Knight GW, Stevens JC, Chum PWS (1993) Elastic substantially linear olefin polymers. US Patent US Patent 5,272,236
- Laun HM (1987) Orientation of macromolecules and elastic deformations in polymer melts. Influence of molecular structure on the reptation of molecules. *Prog Colloid & Polym Sci* 75:111–139. doi:10.1007/BFb0109414
- Lohse DJ, Milner ST, Fetters LJ, Xenidou M, Hadjichristidis N, Roovers J, Mendelson RA, Garcia-Franco CA, Lyon MK (2002) Well-Defined, model long chain branched polyethylene. 2. melt rheological behavior. *Macromolecules* 35(8):3066–3075
- Mavridis H, Shroff RN (1992) Temperature dependence of polyolefin melt rheology. *Polym Eng Sci* 32(23):1778–1791
- Meissner J (1969) Rheometer for the study of mechanical properties of deformation of plastic melts under definite tensile stress. *Rheol Acta* 8(1):78–88
- Meissner J, Hostettler J (1994) A new elongational rheometer for polymer melts and other highly viscoelastic liquids. *Rheol Acta* 33:1–21
- Meissner J, Stephenson SE, Demarmels A, Portmann P (1982) Multiaxial elongational flows of polymer melts—classification and experimental realization. *J Non-Newton Fluid Mech* 11(3–4):221–237

- Münstedt H (1981) The influence of various deformation histories on elongational properties of low density polyethylene. *Colloid Polym Sci* 259:966–972
- Münstedt H, Steffl T, Malmberg A (2005) Correlation between rheological behaviour in uniaxial elongation and film blowing properties of various polyethylenes. *Rheol Acta* 45(1):14–22
- Münstedt H, Kurzbeck S, Stange J (2006) The importance of elongational properties of polymer melts for film blowing and thermoforming. *Polym Eng Sci* 46(9):1190–1195
- Natta G (1963) From the stereospecific polymerization to the asymmetric autocatalytic synthesis of macromolecules. Nobel lecture
- Piel C, Starck P, Seppälä JV, Kaminsky W (2006a) Thermal and mechanical analysis of metallocene-catalyzed ethylene- α -olefin copolymers: the influence of length and number of the crystallizing side-chains. *J Polym Sci A Polym Chem* 44(5):1600–1612. doi:10.1002/pola.21265
- Piel C, Stadler FJ, Kaschta J, Rulhoff S, Münstedt H, Kaminsky W (2006b) Structure-property relationships of linear and long-chain branched metallocene high-density polyethylenes and SEC-MALLS. *Macromol Chem Phys* 207(1):26–38. doi:10.1002/macp.200500321
- Resch JA, Stadler FJ, Kaschta J, Münstedt H (2009) Temperature dependence of the linear steady-state shear compliance of linear and long-chain branched polyethylenes. *Macromolecules* 42(15):5676–5683. doi:10.1021/ma9008719
- Resch JA, Kaschta J, Wolff F, Münstedt H (2011) Influence of molecular parameters on the stress dependence of viscous and elastic properties of polypropylene melts in shear. *Rheol Acta* 50(1):53–63
- Rokudai M, Fujiki T (1981) Influence of shearing history on the rheological properties and processability of branched polymers. 4. Capillary-Flow and Die Swell of low-density polyethylene. *J Appl Polym Sci* 26(4):1343–1350
- Shirayama K, Okada T, Kita S (1965) Distribution of short-chain branching in low-density polyethylene. *J Polym Sci A Polym Chem* 3:907–916
- Sinn H, Kaminsky W (1980) Ziegler-Natta catalysis. *Adv Organomet Chem* 18:99–149
- Stadler FJ (2010) Effect of incomplete datasets on the calculation of continuous relaxation spectra from dynamic-mechanical data. *Rheol Acta* 49(10):1041–1057
- Stadler FJ, Bailly C (2009) A new method for the calculation of continuous relaxation spectra from dynamic-mechanical data. *Rheol Acta* 48(1):33–49. doi:10.1007/s00397-008-0303-2
- Stadler FJ, Karimkhani V (2011) Correlations between terminal rheological quantities and molecular structure in long-chain branched metallocene catalyzed polyethylene. *Macromolecules* 44(13):5401–5413.
- Stadler FJ, Mahmoudi T (2011a) Evaluation of viscosity functions and relaxation spectra of linear and short-chain branched polyethylenes. *J Rheol* (in press)
- Stadler FJ, Mahmoudi T (2011b) Understanding the effect of short-chain branches by analyzing viscosity functions of linear and short-chain branched polyethylenes. *Korea-Australia Rheol J* (in press)
- Stadler FJ, Münstedt H (2008a) Terminal viscous and elastic rheological characterization of ethene- α -olefin copolymers. *J Rheol* 52(3):697–712. doi:10.1122/1.2892039
- Stadler FJ, Münstedt H (2008b) Erratum to “Numerical description of shear viscosity functions of long-chain branched metallocene-catalyzed polyethylenes”. *J Non-Newton Fluid Mech* 151:227. doi:10.1016/j.jnnfm.2008.05.001
- Stadler FJ, Münstedt H (2008c) Numerical description of shear viscosity functions of long-chain branched metallocene-catalyzed polyethylenes. *J Non-Newton Fluid Mech* 151:129–135. doi:10.1016/j.jnnfm.2008.01.010
- Stadler FJ, Münstedt H (2009) Correlations between the shape of viscosity functions and the molecular structure of long-chain branched polyethylene. *Macromol Mater Eng* 294(1):25–34. doi:10.1002/mame.200800251
- Stadler FJ, Kaschta J, Münstedt H (2005) Dynamic-mechanical behavior of polyethylenes and ethene- α -olefin-copolymers: part I: α' -relaxation. *Polymer* 46(23):10311–10320. doi:10.1016/j.polymer.2005.07.099
- Stadler FJ, Piel C, Kaschta J, Rulhoff S, Kaminsky W, Münstedt H (2006) Dependence of the zero shear-rate viscosity and the viscosity function of linear high density polyethylenes on the mass-average molar mass and polydispersity. *Rheol Acta* 45(5):755–764. doi:10.1007/s00397-005-0042-6
- Stadler FJ, Gabriel C, Münstedt H (2007) Influence of short-chain branching of polyethylenes on the temperature dependence of rheological properties in shear. *Macromol Chem Phys* 208(22):2449–2454
- Stadler FJ, Kaschta J, Münstedt H (2008) Thermorheological behavior of long-chain branched metallocene catalyzed polyethylenes. *Macromol* 41(4):1328–1333. doi:10.1021/ma702367a
- Stadler FJ, Becker F, Kaschta J, Buback M, Münstedt H (2009) Influence of molar mass distribution and long-chain branching on strain hardening of low density polyethylene. *Rheol Acta* 48(5):479–490. doi:10.1007/s00397-008-0334-8
- Stadler FJ, Arikian B, Kaschta J, Rulhoff S, Kaminsky W, Münstedt H (2010) Long-Chain Branch Formation in Syndiotactic Polypropylene Induced by Vinyl Chloride. *Macromol Chem Phys* 211:1472–1481. doi:10.1002/macp.200900688
- Stange J, Uhl C, Münstedt H (2005) Rheological behavior of blends from a linear and a long-chain branched polypropylene. *J Rheol* 49:1059–1080
- Stange J, Wächter S, Kaspar H, Münstedt H (2007) Linear rheological properties of the semi-fluorinated copolymer tetrafluoroethylene-hexafluoropropylene-vinylidene fluoride (THV) with controlled amounts of long-chain branching. *Macromol* 40(7):2409–2416. doi:10.1021/ma0626867
- Tackx P, Tacx JCJF (1998) Chain architecture of LDPE as a function of molar mass using size exclusion chromatography and multi-angle laser light scattering (SEC-MALLS). *Polymer* 39(14):3109–3113
- Trinkle S, Walter P, Friedrich C (2002) Van Gorp-Palmen Plot II—Classification of long chain branched polymers by their topology. *Rheol Acta* 41(1–2):103–113
- van Gorp M, Palmen J (1998) Time-temperature superposition for polymeric blends. *Rheol Bull* 67(1):5–8
- Verser DW, Maxwell B (1970) Temperature dependence of low density polyethylene. *Polym Eng Sci* 10(2):122–130
- Wood-Adams PM (1998) The effect of long chain branching on the rheological behavior of polyethylenes synthesized using constrained geometry and metallocene catalysts. Department of Chemical Engineering, Montreal, McGill-University. PhD Thesis
- Wood-Adams PM, Costeux S (2001) Thermorheological behavior of polyethylene: effects of microstructure and long chain branching. *Macromol* 34(18):6281–6290. doi:10.1021/ma0017034
- Ziegler K (1963) Consequences and development of an invention. Nobel lecture
- Zimm BHM, Stockmayer WH (1949) The dimensions of molecules containing branching and rings. *J Chem Phys* 17(12):1301–1314